Arrested Hematopoiesis and Vascular Relaxation Defects in Mice with a Mutation in *Dhfr*

Julie A. I. Thoms,[a] Kathy Knezevic,[a] Jia Jenny Liu,[a] Elias N. Glaros,[b] Thuan Thai,[b] Qiao Qiao,[a] Heather Campbell,[a] Deborah Packham,[a] Yizhou Huang,[a] Peter Papathanasiou,[c] Robert Tunningley,[c] Belinda Whittle,[c] Amanda W. S. Yeung,[b] Vashe Chandrakanthan,[a] Luke Hesson,[a] Vivien Chen,[a,d] Jason W. H. Wong,[a] Louise E. Purton,[e] Robyn L. Ward,[a]* Shane R. Thomas,[b] John E. Pimanda[a,f]

Adult Cancer Program, Prince of Wales Clinical School, Lowy Cancer Research Centre, University of New South Wales, Sydney, NSW, Australia[a]; School of Medical Sciences, University of New South Wales, Sydney, NSW, Australia[b]; Australian Phenomics Facility, John Curtin School of Medical Research, Australian National University, Acton, ACT, Australia[c]; Haematology, Concord Repatriation and General Hospital, Concord, NSW, Australia[d]; Stem Cell Regulation Unit, St. Vincent's Institute of Medical Research and Department of Medicine at St. Vincent's Hospital, The University of Melbourne, Fitzroy, Victoria, Australia[e]; Department of Haematology, Prince of Wales Hospital, Sydney, NSW, Australia[f]

Dihydrofolate reductase (DHFR) is a critical enzyme in the folate metabolism pathway and also plays a role in regulating nitric oxide (NO) signaling in endothelial cells. Although both coding and noncoding mutations with phenotypic effects have been identified in the human *DHFR* gene, no mouse model is currently available to study the consequences of perturbing DHFR *in vivo*. In order to identify genes involved in definitive hematopoiesis, we performed a forward genetic screen and produced a mouse line, here referred to as Orana, with a point mutation in the *Dhfr* locus leading to a Thr136Ala substitution in the DHFR protein. Homozygote Orana mice initiate definitive hematopoiesis, but expansion of progenitors in the fetal liver is compromised, and the animals die between embryonic day 13.5 (E13.5) and E14.5. Heterozygote Orana mice survive to adulthood but have tissue-specific alterations in folate abundance and distribution, perturbed stress erythropoiesis, and impaired endothelium-dependent relaxation of the aorta consistent with the role of DHFR in regulating NO signaling. Orana mice provide insight into the dual roles of DHFR and are a useful model for investigating the role of environmental and dietary factors in the context of vascular defects caused by altered NO signaling.

The primary role of dihydrofolate reductase (DHFR) (5,6,7,8-tetrahydrofolate:NADP$^+$ oxidoreductase; EC 1.5.1.3) is to catalyze the reduction of dietary folate to 7,8-dihydrofolate (DHF) and the subsequent reduction of DHF to 5,6,7,8-tetrahydrofolate (THF). THF, via the actions of a host of other enzymes, is a precursor for 5-methyl THF, which is critical for maintaining DNA methylation, and 5-10-methylene THF, which is required for synthesis of both thymidylate and purine and is thus critical for DNA replication and repair (1). In humans, DHFR-reduced dietary folate is the only source of THF. As such, DHFR is important for ensuring normal DNA synthesis and methylation (1). DHFR also plays a secondary role in nitric oxide (NO) signaling in endothelial cells, where it catalyzes the reduction of dihydrobiopterin (BH2) to tetrahydrobiopterin (BH4), an essential cofactor for endothelial NO synthase (eNOS) (2–4). Reduced intracellular levels of BH4 and/or alteration of the BH4/BH2 ratio in favor of the latter leads to eNOS uncoupling, a process by which eNOS switches from producing the vasoprotective NO to generating the superoxide anion radical ($O_2\cdot^-$) (5), which promotes endothelial dysfunction (6).

Due to its essential role in DNA replication and repair, DHFR is an important target of antineoplastic drugs, such as methotrexate (MTX) (7), and thus, the biochemical properties of DHFR have been studied in relation to normal folate metabolism and in the development of antifolate drugs. Genetic studies have identified both noncoding and coding mutations in the DHFR locus. Noncoding mutations have been described in the promoter, the intronic regions, and the 3′ untranslated region (UTR) (8). The precise roles of these variations are unclear. The best-studied variation is a 19-bp deletion in intron 1 that has been associated with neural tube defects in the offspring of female carriers; however,

multiple studies have produced conflicting results regarding whether this deletion increases or decreases the risk of neural tube defects (9, 10). Other variations have been less well studied but are linked to both cancer susceptibility and resistance to MTX (11–14). Two protein-coding mutations in DHFR have also been described. Patients homozygous for the Leu80Phe mutation (15) had megaloblastic anemia and/or pancytopenia and cerebral folate and BH4 deficiencies, while patients homozygous for the Asp153Val mutation (16) had megaloblastic anemia and mild learning disabilities.

However, despite the critical roles of DHFR and folate metabolism in human health and disease, no animal models are currently available to study the effect of null or loss-of-function DHFR alleles on normal development and tissue homeostasis. Cell line models are also limited in their capacity to yield insights into tissue- and locus-specific aberrations in DNA methylation

and cancer susceptibility in the presence of persistent abnormalities in tissue folate metabolism.

Ethylnitrosourea (ENU) mutagenesis is a powerful tool for generating point mutations in mice that can then be screened for phenotypic effects (17). Such screens have the advantage of potentially generating loss- or gain-of-function alleles, as opposed to knockout mice, which are generally limited to removing a functional allele. In this study, we describe a mouse generated through an ENU mutagenesis screen followed by extensive backcrossing, with a single point mutation in the *Dhfr* locus leading to a Thr136Ala substitution in the DHFR protein. Homozygote animals die of blood defects between embryonic day 13.5 (E13.5) and E14.5, while heterozygote adults survive with a relatively intact blood compartment but show tissue-specific defects in distribution of folate species and impaired stress-induced hematopoiesis and blood vessel relaxation.

MATERIALS AND METHODS

Generation of mice, phenotyping, and mapping. The Orana (Ora) mouse line was generated by ENU mutagenesis followed by a screen for recessive hematopoietic phenotypes, as described previously (18). Briefly, fetal livers (FLs) from E14.5 embryos were screened by flow cytometry in order to enumerate six distinct hematopoietic stem cell (HSC) and progenitor subsets (long-term hematopoietic stem cells [LT-HSCs], multipotent progenitors [MPPs], common lymphoid progenitors [CLPs], common myeloid progenitors [CMPs], granulocyte/macrophage progenitors [GMPs], and megakaryocyte/erythrocyte progenitors [MEPs]), and fetal blood (FB) from E14.5 embryos was screened by flow cytometry to enumerate yolk sac-derived primitive red blood cells (RBCs), FL-derived definitive RBCs, and platelets. For linkage analysis, genomic DNA from 7 affected and 12 unaffected F2 C57BL/6J × C57BL/10SnJ mice was screened with approximately 80 strain-specific single nucleotide polymorphism (SNP) markers spaced at 20- to 30-Mb positions on each chromosome using the Amplifluor SNP genotyping system (Chemicon, Millipore). The Orana causal mutation was mapped to a region on chromosome 13 between bases 66366699 and 101979187 (mm9), which contained 307 genes. Of these, three candidate genes (*Mtrr* [ENSMUSG00000034617], *Dhfr* [ENSMUSG00000021707], and *Tert* [ENSMUSG00000021611]) with known or suspected roles in blood development were selected for sequence analysis. Sequencing of the candidate genes was performed to locate the causal ENU base substitution, and DNA was prepared from an individual affected mouse. Primers were designed for candidate genes to amplify all exons by ±15 bp to cover splice junctions. The amplicons were then Sanger sequenced on an Applied Biosystems 3730*xl* capillary sequencer. This automated platform uses Big-Dye Terminator (BDT) chemistry version 3.1 (Applied Biosystems). The raw trace files were analyzed using Lasergene software (DNAStar) against the C57BL/6 mouse reference genome (NCBI). Using this approach, a single base substitution (A to G) of base pair 885 in exon 5 (ENSMUSE00000120178) was detected in *Dhfr*. This mutation results in an ACA (Thr)-to-GCA (Ala) change of amino acid 136. All animal experiments were performed with approval from the University of New South Wales Animal Ethics committee.

Primers and antibodies. The PCR primers used were as follows: for genotyping, Orana-1 (5′-GAAGGTCGGAGTCAACGGATTCTTTCAAA TTCCTGCATGATCCTTGT-3′), Orana-2 (5′-GAAGGTGACCAAGTT CATGCTCAAATTCCTGCATGATCCTTGC-3′), and Orana-R (5′-GAG GAGAGTGATACCTTGTGTT-3′); for expression, mDHFR F (5′-GTAG AGAACTCAAAGAACCACCAC-3′), mDHFR R (5′-CAGAACTGCCTC CGACTATCC-3′), mB2M F (5′-GAGACTGATACATACGCCTGCAG A-3′), and mB2M R (5′-TCACATGTCTCGATCCCAGTAGA-3′); for cloning and mutagenesis, mut hDHFR F (5′-CAGGCCATCTTAAACTA TTTGTGGCAAGG-3′), mut hDHFR R (5′-CACTTTCAAAGTCTTGCA TGATCCTTGCCAC-3′), hDHFR F (5′-TCCCGGGTCATGGTTGGTT

CGCTAAACTGC-3′), hDHFR F2 (5′-TCCCGGGTATGGTTGGTTCGC TAAACTGC-3′), and hDHFR R (5′-GTCGACCTCGAGTATTAATCAT TCTTCTCATATAC-3′); for sequencing, hDHFR seq 1 (5′-CGCTGTGT CCCAGAACATGGGC-3′), hDHFR seq 2 (5′-GCCTTTCTCCTCCTGG ACATC), mDHFR seq 1 (5′-CTGCCTTTCAGCACAGGTTG-3′), and mDHFR seq 2 (5′-TTACTTGCTTCCCCTTCTTTCTG-3′); for pyrosequencing, mKcnq1ot1 F (5′-GYGYGGGTTTTTTTTTTGAGTTAGT), mKcnq1ot1 R 5′ biotinylated (5′-CRATATCCTAAACCACTCACCTTA-3′), and mKcnq1ot1 sequencing (5′-GTTAGAAGTAGAGGTGAT-3′).

The antibodies used were as follows: from Abcam, anti-DHFR (ab133546); from BD, streptavidin-phycoerythrin-Texas red (551487), anti-mouse CD117–allophycocyanin (APC) H7 (560250), anti-mouse Ly-6A/E V500 (561229), anti-mouse CD34–fluorescein isothiocyanate (FITC) (553733), anti-mouse CD135–APC (560718), anti-mouse CD127–phycoerythrin (PE) (552543), anti-mouse Ter119–PE (553673), and 7-aminoactinomycin D (7-AAD) (559925); from BioLegend, anti-mouse CD48 BV421 (103427) and anti-mouse CD150 (SLAM)–PE–Cy5 (115911); and from eBiosciences, anti-mouse CD16/32–PE-Cy7 (25-0161-81), anti-mouse CD3e–biotin (13-0031), anti-mouse CD4–biotin (13-0041), anti-mouse CD5–biotin (13-0051), anti-mouse CD8a–biotin (13-0081), anti-mouse CD45R/B220–biotin (13-0452), anti-mouse Ly-6G (Gr-1)–biotin (13-5931), anti-mouse CD11b (Mac-1)–biotin (13-0112), anti-mouse Ter119–biotin (13-5921), anti-mouse CD44–APC (17-0441-81), and anti-mouse CD177 (cKit)–APC-eFluor780 (47-1171-80).

DNA and RNA isolation, cDNA synthesis, and qPCR. Genomic DNA was prepared by proteinase K digestion of tissue and DNA. RNA was prepared using the RNeasy minikit (Qiagen), and cDNA was synthesized using standard protocols. Quantitative PCR (qPCR) was performed using SYBR green ER (Life Technologies) and an MX3000P thermocycler (Agilent).

Protein isolation and Western blotting. Liver tissue for the DHFR activity assay was homogenized in buffer (75 mM MnCl$_2$, 2 mM dithiothreitol [DTT], 1 mM EDTA plus protease inhibitors) and centrifuged at $17,000 \times g$ for 45 min, and the supernatant was stored at $-80°C$. The protein concentration was estimated by Bradford assay (Bio-Rad).

Cells and tissue for Western blotting were solubilized in RIPA buffer (50 mM Tris-HCl, pH 7.4, 150 mM NaCl, 1% Triton X-100, 0.5% sodium deoxycholate, 0.1% SDS, 1 mM EDTA) plus protease inhibitors, boiled in sample buffer plus DTT, resolved in 4 to 12% Bis-Tris gels in MOPS (4-morpholinepropanesulfonic acid) buffer (Novex), and transferred to nitrocellulose membranes. The membranes were probed with antibodies against DHFR or β-actin, followed by secondary antibody, and developed with Luminol reagent (Santa Cruz). Bands were detected using an ImageQuant LAS4000 and quantified using ImageQuant software (GE).

DHFR expression vectors. The human DHFR cDNA was donated by Tseng Ting Kao (National Cheng Kung University, Taiwan). Site-directed mutagenesis was performed to introduce the Orana mutation. The DHFR cDNA was PCR amplified and subcloned into either pGEX-6P-1 or pcDNA3.

DHFR activity assay. Twenty microliters of liver lysate or recombinant protein was added to 200 μl of buffer (0.1 M potassium phosphate, pH 7.4, 0.5 M KCl, 1 mM EDTA, 1 mM DTT, 20 mM sodium ascorbate) and incubated for 9 min at 37°C, and then 150 μM NADPH was added for an additional minute. Dihydrofolic acid (Sigma) was added to a final concentration of 87 μM and incubated for 2 min. Reactions were stopped by adding an equal volume of 0.5 M perchloric acid. Samples were centrifuged at $500 \times g$ for 2 min at 4°C and then filtered through a Chromadisk 4A microfilter and measured by high-performance liquid chromatography (HPLC) and electrochemical detection (ECD) as described previously (19).

Production of recombinant protein. pGEX-6P-1 DHFR-transformed BL21 competent cells were grown to an optical density at 600 nm (OD$_{600}$) of 0.5 and induced with 0.15 mM isopropyl-β-D-thiogalactopyranoside (IPTG) for 4 h at 30°C. EDTA (1 mM final concentration) was added to stop the induction. The cells were pelleted and washed in phos-

phate-buffered saline (PBS) and then lysed with buffer (50 mM Tris, pH 7.5, 150 mM NaCl, 5 mM EDTA, 0.5% NP-40, 1% Triton X-100, 10 mM DTT plus protease inhibitors), sonicated, and centrifuged at 5,000 × g for 15 min at 4°C. The supernatant was incubated with glutathione S-transferase (GST) beads (Roche) for 1 h and washed twice in PBS–1% Triton X-100, and the purified protein was eluted with 100 mM Tris, pH 7.5, 20 mM NaCl, 10 mM glutathione.

Expression of DHFR in 293T cells. 293T cells were grown in Dulbecco's modified Eagle's medium (DMEM) containing 10% fetal bovine serum (FBS). The cells were transfected using Lipofectamine 2000 (Life Technologies) according to the manufacturer's instructions; 24 h after transfection, the cells were treated with 1 μM bortezomib (BTZ) (Janssen-Cilag) for a further 24 h and then harvested in RIPA buffer supplemented with protease inhibitors.

Measurement of folate species. The concentrations and distributions of folate species were measured in 2 homozygous (Ora/Ora), 6 heterozygous (+/Ora), and 3 wild-type (WT) (+/+) E13.5 embryonic livers and in the remaining embryonic tissue (whole embryos). Folate was also measured in six tissues (liver, brain, bone marrow [BM], aorta, colon, and small intestine) in one +/+ and two +/Ora adult mice. Where available, 100 mg of tissue was used for folate extraction; otherwise, 20 mg of tissue was used, and the scale-down protocol for folate extraction was applied as previously described (20, 21). The extraction of five folate species (THF, folic acid, 5-methyl THF, 5-formyl THF, and 5,10-methenyl THF) from tissues, purification by solid-phase extraction, and measurement using liquid chromatography tandem mass spectrometry (LC–MS-MS) were performed using a validated method, as previously described (21).

Measurement of global DNA methylation. 5-Methyl-2′-deoxycytidine (5mdC) was determined as a percentage of 2′-deoxycytidine plus 5mdC in genomic DNA using stable-isotope dilution LC–MS-MS based upon the method of Quinlivan and Gregory (22). In brief, this method involves the in-house biosynthesis of $[^{15}N_3]$deoxycytidine ($[^{15}N_3]$dC) and $[^{15}N_3]$5mdC internal standards and one-step digestion of 1 μg genomic DNA spiked with U-^{15}N-labeled internal standards into deoxyribonucleosides (23). Genomic DNA was extracted from mouse whole-embryo and adult tissues using phenol-chloroform-isoamyl alcohol and quantified by measuring the UV absorbance at 260 nm (NanoDrop 1000; NanoDrop Technologies Inc.). Purity was confirmed by a 260/280 ratio of >1.8; 500 ng was used for the assay. The conditions for ultra-high-performance liquid chromatography (UHPLC) and the triple-quadrupole mass spectrometer have been previously reported (20). Analyses were performed using an ultra-high-performance liquid chromatography Accela Pump (Thermo Finnigan) and an HTC PAL (CTC Analytics) autosampler coupled directly to a TSQ Quantum Access triple-quadrupole mass spectrometer (Thermo Finnigan) in the positive-ion mode via an electrospray interface. LC was performed on an Acquity UHPLC HSS T3 column (2.1 by 100 mm; 1.8 μm). Twenty microliters of the sample was analyzed using gradient elution with aqueous 0.1% formic acid (solvent A) and acetonitrile (solvent B) at a flow rate of 0.4 ml/min over 7 min. The acetonitrile gradient increased linearly from 0% at 0.7 min to 22.5% at 3.5 min, at which time it was ramped up to 100% by 3.85 min and held for 0.55 min before being returned to baseline at 4.55 min. The mass-to-charge transitions of the analytes monitored were identical to those used by Quinlivan and Gregory (22). Data were processed using the Quanbrowser function of the Xcalibur software package v2.0.7. In-house method validation was performed as previously described (20). Four quality control samples with known global DNA methylation levels (two from human peripheral blood DNA and two from colorectal cancer cell lines) and one blank sample were run with each batch of samples to check for interbatch variation and to blank for unlabeled analytes in the internal standard mixture (this was always <0.1%).

Measurement of DNA methylation by bisulfite pyrosequencing. The DNA samples for bisulfite pyrosequencing were the same as those used for measurement of global DNA methylation. Sodium bisulfite modification

was performed using the EZ DNA Methylation-Gold kit (Zymo Research) according to the manufacturer's instructions. Region 4 for the *Kcnq1ot1* CpG island (24) was amplified from 100 ng of bisulfite-treated DNA using primers mKcnq1ot1 F and mKcnq1ot1 R. The biotinylated bisulfite-modified PCR products were sequenced using the mKcnq1ot1 sequencing primer on a PyroMark Q24 pyrosequencer (Qiagen) and analyzed using the PyroMark Q24 Advanced version 3.0 software. Methylation levels at each CpG site were measured in triplicate in each tissue.

Homocysteine measurement. Blood from adult +/+ and +/Ora mice was obtained by cardiac puncture. Plasma homocysteine levels were determined using standard clinical testing parameters (25–28) and a Shimadzu LC-20 HPLC and ABSciex 4000 QTrap MS.

Whole mounts, tissue sections, and staining. Embryos were harvested at E11.5 and E13.5, fixed, embedded in paraffin, sectioned, and counterstained with neutral red. Images were acquired with a Leica DFC 420C digital camera attached to either a Leica S8APO or DM2500 microscope, using the Leica Application Suite.

In vitro **colony assays.** Colony assays were performed in triplicate in Methocult GF-3434 (Stemcell Technologies). For FL, triplicate dishes were seeded with 10,000 liver cells. For the aorta-gonad-mesonephros (AGM) region, the entire AGM was dissociated into single cells and seeded across 3 dishes. Colonies (burst-forming unit-erythroid [BFU-E], CFU-granulocyte, macrophage [CFU-GM], and CFU-granulocyte, erythroid, macrophage, megakaryocyte [CFU-GEMM]) were scored after 9 to 11 days.

Flow cytometry. For analysis of progenitor cells, mononuclear cells from +/+ and +/Ora adult BM were isolated by Ficoll separation prior to staining. For analysis of erythroid maturation, femurs were flushed with PBS containing 5% bovine serum albumin (BSA) and 2 mM EDTA (fluorescence-activated cell sorter [FACS] buffer), and the spleens were crushed in FACS buffer prior to staining and analysis. For FL analysis, the entire FL from E13.5 and E11.5 +/+, +/Ora, and Ora/Ora mice was crushed in FACS buffer prior to staining and analysis. The stained cells were analyzed using either an LSR Fortessa SORP cell analyzer or a FACS Canto II analyzer (both BD Biosciences, San Jose, CA).

For analysis of erythroid maturation, cells were first gated as 7-AAD negative (live) and Ter119 positive, and the resulting population was plotted as CD44 versus forward scatter (FSC). Regions representing six erythroid populations (proerythroblasts [I], basophilic erythroblasts [II], polychromatic erythroblasts [III], orthochromatic erythroblasts [IV], reticulocytes [V], and RBCs [VI]) were drawn essentially as described by Liu et al. (29).

5-Fluorouracil hematoablation. Age-matched +/+ and +/Ora mice were injected intraperitoneally with 5-fluorouracil (5FU) (Hospira Australia) at 150 mg/kg of body weight. Minimal submandibular blood samples were taken weekly, diluted in PBS, and analyzed using an Ac · T Diff analyzer (Beckman Coulter) using equine settings. Undiluted blood was smeared on slides, dried, and stained with Wright's stain. Twenty-eight days following injection, the mice were culled, and the spleens and bone marrow were collected for flow cytometry analysis of developing erythroid populations.

Vascular-function assay. Aortas were harvested from age-matched +/+ or +/Ora mice (age, 10 to 44 weeks) and placed into prechilled modified Krebs-Henseleit (KH) buffer (NaCl, 118.4 mmol/liter; KCl, 4.7 mmol/liter; $CaCl_2$, 2.5 mmol/liter; $MgSO_4$, 1.2 mmol/liter; KH_2PO_4, 1.2 mmol/liter; $NaHCO_3$, 25.0 mmol/liter; EDTA, 0.023 mmol/liter; and glucose, 11.1, mmol/liter; pH 7.4). Perivascular adipose and connective tissues were carefully removed from the thoracic aorta, which was cut into rings 2 mm thick. The aortic rings were then mounted in individual organ chambers of a Myograph system (MultiMyograph 610M; Danish Myo Technology, Aarhus, Denmark) containing 6 ml of KH buffer equilibrated with carbogen gas (95% O_2-5% CO_2) and maintained at 37°C. Isometric tension was monitored with a force transducer connected to a data acquisition system. The tension on each vessel segment was slowly increased until it reached a resting or baseline tension of 9.8 mN, which
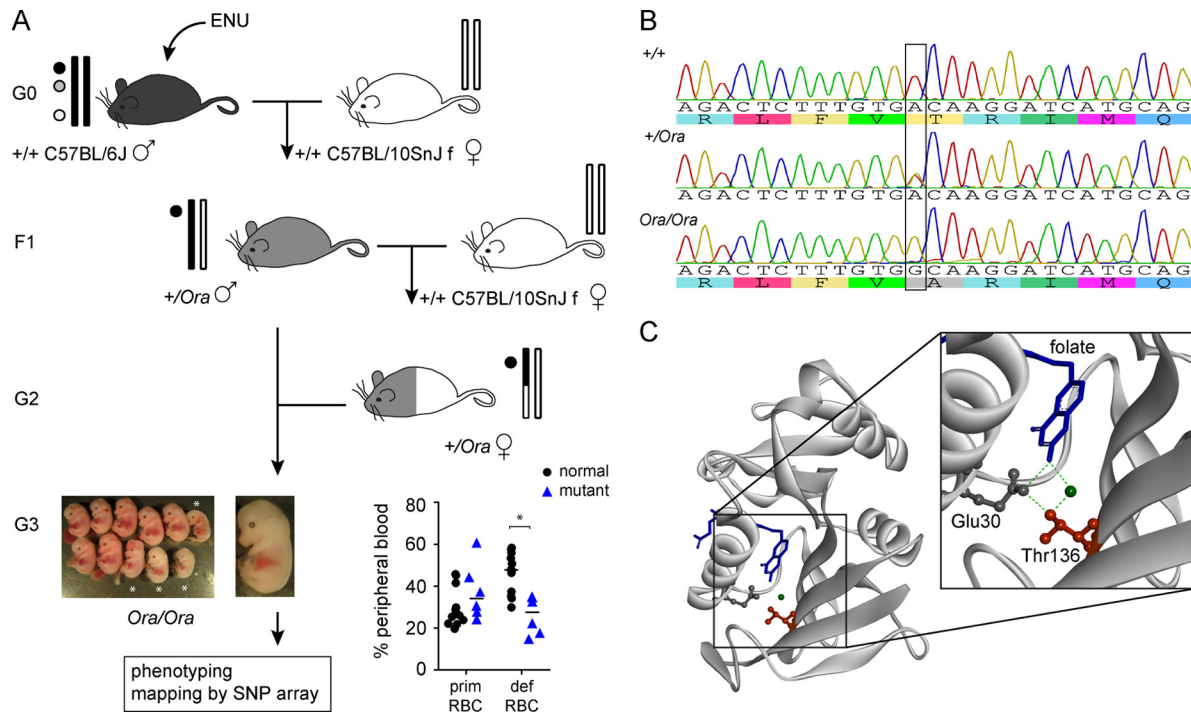
FIG 1 Orana mice have a point mutation in *Dhfr*, the gene encoding dihydrofolate reductase. (A) Schematic showing the ENU mutagenesis and screening strategy that led to the discovery of the Orana phenotype. The graph shows primitive (prim) RBCs and definitive (def) RBCs in blood from phenotypically normal (normal) and phenotypically mutant (mutant) E14.5 embryos. *, $P < 0.001$; *t* test. The bars in the graphs indicate the medians. (B) Sanger sequencing of +/+, +/Ora, and Ora/Ora mice showing a single A-G mutation at chromosome 13 base 92368224 (mm10). This mutation leads to an altered amino acid sequence of the DHFR protein (Thr136Ala). (C) Structure diagram (derived from Protein Data Bank [PDB] 4M6K [32]) showing human DHFR (gray) bound to folate (blue) and NADPH (not shown), indicating the position of Thr136 (red) in the folded protein. The dotted green lines indicate observed hydrogen bonds between Thr136, Glu30 (dark gray), water (green circle), and folate (30–32).

was maintained throughout the remainder of the study. After a 15-min equilibration period, the segments were stretched to their optimal passive tension by the response to 125 mM KCl, which induced maximal vessel contraction. Once the tension reached a plateau, the segments were washed 4 times with regular KH buffer over 5 min. This KCl contraction/wash step was repeated twice. After 30 min equilibration, the aortic rings were placed in KH buffer supplemented with indomethacin (10 μmol/liter to inhibit cyclooxygenase and the synthesis of vasoactive prostanoids) and contracted with phenylephrine until a stable contraction plateau of approximately 80% of maximal tension (achieved with 125 mM KCl) was reached. The concentration-dependent vascular-relaxation responses induced by the endothelium-dependent dilator acetylcholine (Ach) (1 nmol/liter to 1 μmol/liter) were then recorded. Endothelium-independent responses were recorded in response to the NO donor diethylammonium (*Z*)-1-(*N*,*N*-diethylamino)diazen-1-ium-1,2-diolate (DEANO) (1 nmol/liter to 10 μmol/liter). Vasorelaxation responses were expressed as the percent relaxation of the submaximal contraction in response to phenylethrine. To examine the effect of sepiapterin supplements on vascular reactivity, aortic rings were incubated with or without sepiapterin (100 μM) for 60 min at 37°C in 1 ml KH buffer in Eppendorf tubes and subsequently mounted for myography.

RESULTS

Orana mice have a point mutation in *Dhfr*, the gene encoding dihydrofolate reductase. We used a recently described method (18) to carry out a forward recessive genetic screen in mice to identify genes involved in definitive hematopoiesis. G3 (Fig. 1A) offspring of ENU-mutagenized males were screened at E14.5 for altered distributions of hematopoietic populations. Some em-

bryos from pedigree 25 of this screen were small and pale (Fig. 1A; G3 phenotypically homozygote embryos are indicated by asterisks); this line was named Orana (Ora), in line with the naming convention of the Australian Phenomics Facility, where the line was generated (18). All three genotypes were present at roughly Mendelian ratios in E13.5 embryos (26:55:19; *n* = 84); however, homozygosity for the Orana allele was embryonic lethal soon after E14.5. Flow cytometry analysis of blood from phenotypically mutant embryos indicated a moderate increase in primitive RBCs and a significant decrease in definitive RBCs (Fig. 1A). There was also an increase in cKit$^+$ Sca1$^-$ and cKit$^+$ Sca1$^+$ lin$^-$ (LSK) cells in G3 mice, although this phenotype was not observed following extensive backcrossing onto a C57BL/6J background (all data are expressed as median percent LSK cells in nucleated FL, range, and *n*): E14.5 G3 mice, phenotypically normal (0.74, 0.27 to 1.12, 14) and phenotypically mutant (2.28, 0.92 to 3.18, 5) ($P < 0.001$; *t* test); E13.5 backcrossed mice, +/+ (0.475, 0.22 to 3.41, 8), +/Ora (0.535, 0.19 to 1.39), and Ora/Ora (0.55, 0.34 to 0.078, 4). Together, these data suggest that the gene responsible for the Orana phenotype plays a role in early blood development. After extensive backcrossing, the Orana mutation was mapped by SNP array and candidate sequencing to exon 5 of the *Dhfr* gene on chromosome 13. A single A-to-G mutation was observed at chromosome 13 base 92368224 (mm10) (Fig. 1B), which led to the replacement of Thr136 with Ala. The crystal structure of DHFR coupled with folic acid and NADPH indicates that OG1 of Thr136 is hydrogen bonded to the pteridine moiety of folate through an intervening
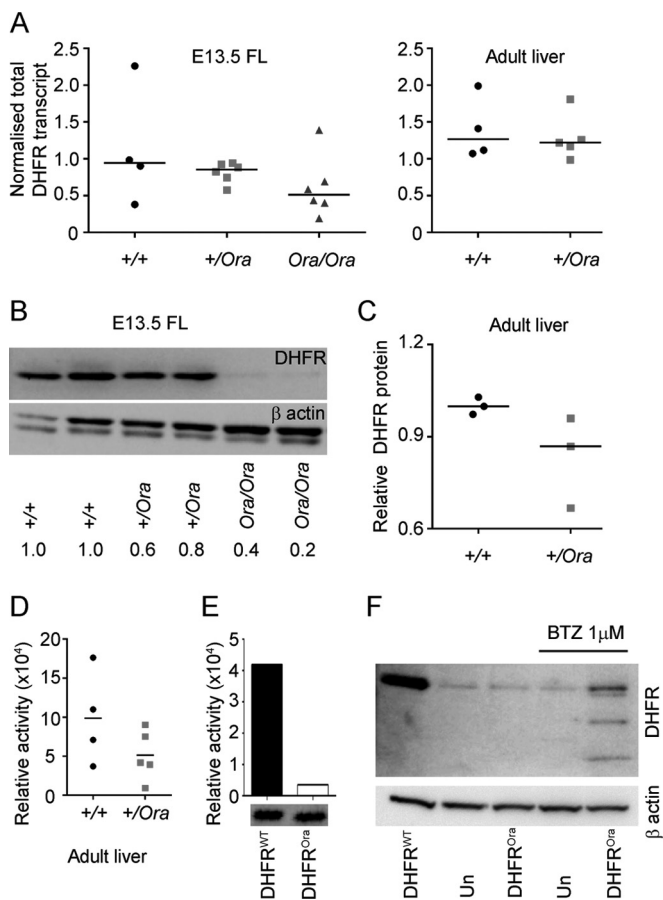
ity was detected for recombinant DHFR^{WT} protein, DHFR^{Ora} was essentially unable to catalyze the NADPH-dependent conversion of DHF to THF (Fig. 2E, top). The anti-DHFR antibody detected low levels of DHFR in the Ora/Ora mice and recognized both WT (DHFR^{WT}) and Orana (DHFR^{Ora}) recombinant proteins (Fig. 2E, bottom), so it is unlikely that the reduced DHFR expression observed in Ora/Ora embryos was due to impaired antibody affinity for the DHFR^{Ora} protein. Rather, these data suggest that the mutant DHFR^{Ora} was synthesized and subsequently degraded, potentially due to misfolding. We tested this hypothesis directly by expressing DHFR^{WT} and DHFR^{Ora} in 293T cells (Fig. 2F). At 24 h after transfection, DHFR^{WT} was readily detectable by Western blotting. In contrast, no DHFR^{Ora} could be detected above endogenous background. However, treatment of DHFR^{Ora}-transfected cells with the proteasomal inhibitor BTZ resulted in increased DHFR expression and the appearance of partial degradation products, indicating that the DHFR^{Ora} protein was degraded via the proteasome.

Homozygous Orana embryos have defects in folate metabolism consistent with reduced DHFR activity. Having found that animals harboring the Orana allele had reduced levels of functional DHFR, we next investigated the consequences of this defect for folate metabolism. The Orana mutation in DHFR is expected to impair reduction of dietary folic acid into THF and the subsequent availability of folate species for methylation reactions (via 5-methyl THF) and DNA synthesis (via 5,10-methylene THF and 5-formyl THF [Fig. 3A]). E13.5 Ora/Ora embryos contained on average less than half the total tissue folate concentration of +/+ and +/Ora embryos (Fig. 3B). The 5-methyl THF concentration was 9-fold lower while the folic acid concentration was 15-fold higher in Ora/Ora embryos compared to +/+ embryos (Fig. 3B). This resulted in a substantially perturbed tissue folate distribution in Ora/Ora embryos compared to +/+ embryos, with a reduced proportion of 5-methyl THF and an increased proportion of unmetabolized folic acid, 5,10-methenyl THF, and 5-formyl THF for DNA synthesis (Fig. 3C). This shift in folate distribution is consistent with the impaired ability of folic acid to be reduced by DHFR into metabolically active forms. Despite the reduced availability of 5-methyl THF, a methyl donor required for DNA methylation, no significant differences in global DNA methylation (Fig. 3D, left), or methylation of a CpG island adjacent to the promoter of a known imprinted gene, Kcnq1ot1, was detected in Ora/Ora embryos compared to +/+ and +/Ora embryos (Fig. 3D, right).

In addition to whole embryos, we analyzed the folate concentration and distribution in E13.5 embryonic livers. Similar reductions in total folate, 5-methyl THF, and THF concentrations were found in the embryonic livers of Ora/Ora mice compared to +/+ mice (Fig. 4A). The overall distribution of folate species in the embryonic liver was also perturbed (Fig. 4B).

Interestingly, no significant differences in the whole embryo or liver tissue folate concentration or species distribution was found in +/Ora compared to +/+ samples, which suggested that a single WT allele of Dhfr was adequate to sustain folate metabolism of the embryo in vivo. To determine whether the folate concentration was also sustained in adult +/Ora mice compared to +/+ mice, we profiled tissue folate species and DNA methylation in six tissues from one adult +/+ mouse and two +/Ora mice. We found that the total folate concentrations in the BM of both +/Ora mice were half that of the +/+ mouse, although folate species distributions were similar (Fig. 4C). Folate concentrations and distribu-

FIG 2 Mice harboring the Orana (Ora) allele have reduced levels of functional DHFR. (A) Relative mRNA expression in +/+, +/Ora, and Ora/Ora E13.5 fetal liver and in +/+ and +/Ora adult livers. (B) Protein expression in +/+, +/Ora, and Ora/Ora E13.5 fetal liver. The numbers indicate DHFR protein levels normalized to β-actin. (C) Relative DHFR protein expression in +/+ and +/Ora adult livers. (D) DHFR activity of equal amounts of protein from +/+ and +/Ora adult livers. (E) DHFR activity and Western blot of equal amounts of recombinant WT (DHFR^{WT}) and Orana (DHFR^{Ora}) DHFR protein expressed in E. coli. (F) Ectopic expression of WT and Orana DHFR in 293T cells before and after treatment with the proteasomal inhibitor BTZ. The bars in all the graphs indicate the medians.

water molecule (Fig. 1C) (30–32). OG1 is absent in Ala, so the Thr136Ala mutation is predicted to alter the affinity of DHFR for folic acid and therefore to compromise enzyme function.

The Orana mutation compromises the catalytic activity and protein stability of DHFR. WT (+/+), heterozygous (+/Ora), and homozygous (Ora/Ora) E13.5 FLs all expressed DHFR mRNA at comparable levels, and no difference in expression levels was observed in adult +/+ versus +/Ora livers (Fig. 2A). However, a reduction in total DHFR protein was observed in +/Ora E13.5 livers, while DHFR was barely detectable in Ora/Ora E13.5 livers (Fig. 2B). A modest reduction in DHFR levels was observed in heterozygote adult livers (Fig. 2C), and DHFR activity was also reduced in +/Ora compared to +/+ adult livers (Fig. 2D). DHFR protein was essentially undetectable in Ora/Ora embryos and had reduced expression in +/Ora embryos and adults, so we asked whether the Thr136Ala mutation itself altered DHFR activity. Recombinant DHFR^{WT} and DHFR^{Ora} proteins were readily expressed in Escherichia coli (Fig. 2E, bottom). While enzyme activ-
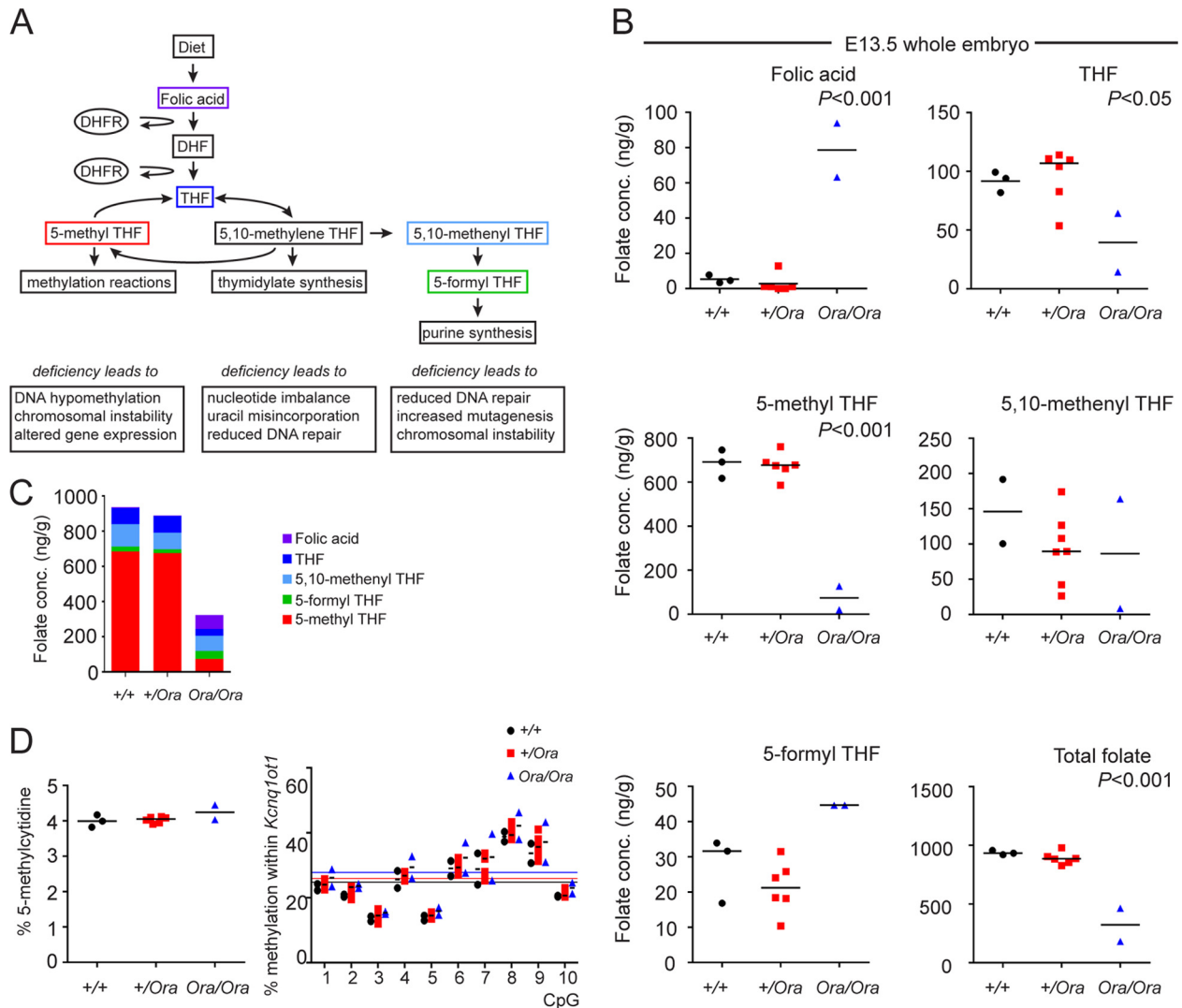
FIG 3 Homozygous Orana embryos have defects in folate metabolism consistent with reduced DHFR activity. (A) Simplified flow chart of folate-mediated one-carbon metabolism illustrating the roles of different folate species. Dietary folic acid is reduced by the enzyme DHFR to DHF and THF. THF is converted to 5,10-methylene THF, an essential precursor for thymidylate synthesis, which is the rate-limiting step in DNA synthesis. 5,10-Methenyl THF and 5-formyl THF play important roles in purine synthesis. The recycling of 1 carbons back to THF occurs via 5-methyl THF, which is a critical folate species for methylation reactions, particularly DNA methylation. The consequences of a deficiency or imbalance of folate species are summarized. (B) Concentrations of folate species in +/+ (*n* = 3), +/Ora (*n* = 6), and Ora/Ora (*n* = 2) E13.5 whole embryos. *P* values are indicated (one-way analysis of variance [ANOVA]). (C) Overall abundance and distribution of folate species in E13.5 whole embryos. (D) DNA methylation levels in E13.5 whole embryos. (Left) Global. (Right) At individual CpGs adjacent to the *Kcnq1ot1* promoter. The horizontal lines indicate mean methylation levels across all 10 CpGs for +/+ (black line; mean = 24.76%), +/Ora (red line; mean = 25.92%), and Ora/Ora (blue line; mean = 27.75%). The bars in all the plots indicate the medians.

tions in other tissues, including aorta, liver, small intestine, colon, and brain, were identical (Fig. 4C and data not shown). Moreover, global DNA methylation (Fig. 4D and data not shown) and methylation of a CpG island adjacent to the promoter of a known imprinted gene, *Kcnq1ot1* (Fig. 4E and data not shown), in the adult +/+ tissues were similar to those in +/Ora mice. In some tissues, we did observe a small increase in average methylation across the *Kcnq1ot1* CpG island (e.g., the liver panel in Fig. 4E); however, when taken together, our data indicate that decreased DHFR expression does not lead to substantial changes in either global methylation or methylation at the imprinted *Kcnq1* gene.

We also measured plasma homocysteine levels in adult mice, since recycling of homocysteine to methionine via methionine synthase requires a methyl group usually donated by the conversion of 5-methyl THF to THF (33). Consistent with our direct measurement of folate species and global DNA methylation, we observed no significant difference in plasma homocysteine concentration between +/+ and +/Ora mice (data not shown).

Reduced DHFR function leads to defects in embryonic blood production. Having originally identified the Orana line based on its recessive blood phenotype, we further characterized the phenotype in Ora/Ora embryos. At E11.5, the gross morphologies of +/+, +/Ora, and Ora/Ora embryos were similar, although the livers of Ora/Ora mice appeared slightly paler (Fig. 5A, top). In contrast, at E13.5, Ora/Ora embryos were smaller and paler than their +/+ littermates (Fig. 5B, top, and C). The fetal liver is the
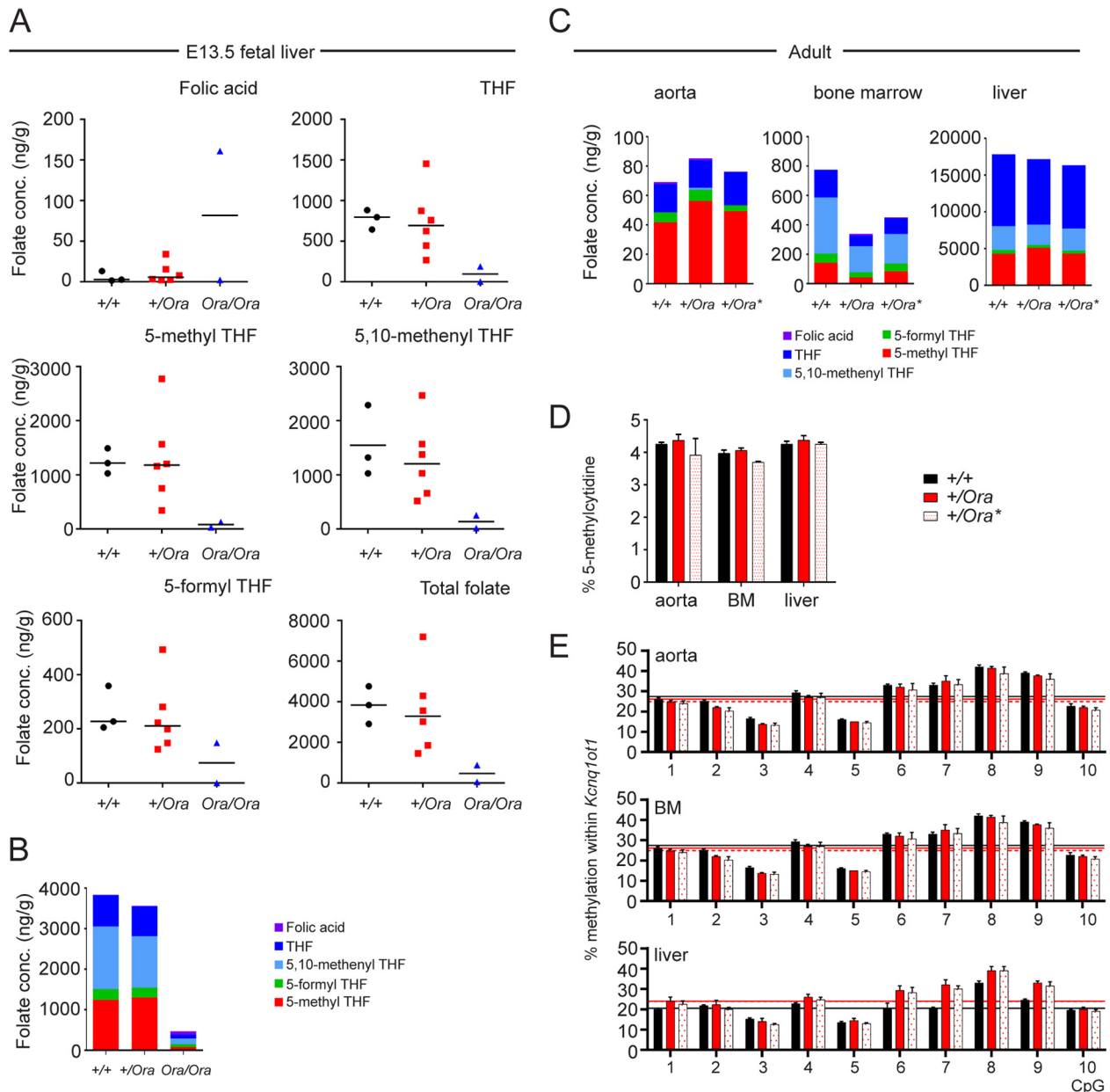
FIG 4 Homozygous Orana FLs have defects in folate metabolism consistent with reduced DHFR activity, while adult heterozygotes have altered folate metabolism in a subset of tissues. (A) Concentrations of folate species in +/+ (n = 3), +/Ora (n = 6), and Ora/Ora (n = 2) E13.5 livers. The bars in the graphs indicate the medians. (B) Overall abundance and distribution of folate species in E13.5 livers. (C) Overall abundance and distribution of folate species in adult aorta, bone marrow, and liver, *, pregnant +/Ora mouse. (D) Global DNA methylation level in adult aorta, bone marrow, and liver. (E) Methylation of individual CpGs adjacent to the *Kcnq1* promoter in adult aorta, bone marrow, and liver. The horizontal lines indicate mean methylation across all 10 CpGs for +/+ (black line; aorta mean = 27.43%, BM mean = 23.6%, and liver mean = 20.52%), +/Ora (red line; aorta mean = 26.11%, BM mean = 24.26%, and liver mean = 24.00%), and pregnant +/Ora (dashed red line; aorta mean = 24.97%, BM mean = 25.63%, and liver mean = 24.02%). The error bars indicate standard errors of the means (SEM).

primary hematopoietic organ at E11.5, having been seeded by HSCs formed in the AGM (34–36). Close inspection of the E11.5 liver revealed a reduction in erythrocytes in Ora/Ora mice (Fig. 5A, bottom), indicating that reduced DHFR led to reduced blood production. A reduction in erythrocytes was also observed in E13.5 livers (Fig. 5B, bottom). This is consistent with the reduction in definitive RBCs observed during the initial ENU mutagenesis screen (Fig. 1A). We next assessed whether blood progenitors

from the FL and AGM were functional using colony assays. At E11.5, there was a significant decrease in BFU-E, CFU-GM, and CFU-GEMM colonies in Ora/Ora embryos (Fig. 6A), which indicated a reduced number of functional progenitor cells in the rapidly expanding hematopoietic FL compartment. In contrast, progenitor cells in the AGM of Ora/Ora embryos were able to generate BFU-E and CFU-GM colonies, although the numbers of the more primitive CFU-GEMM colonies were reduced (Fig. 6B). BFU-E and
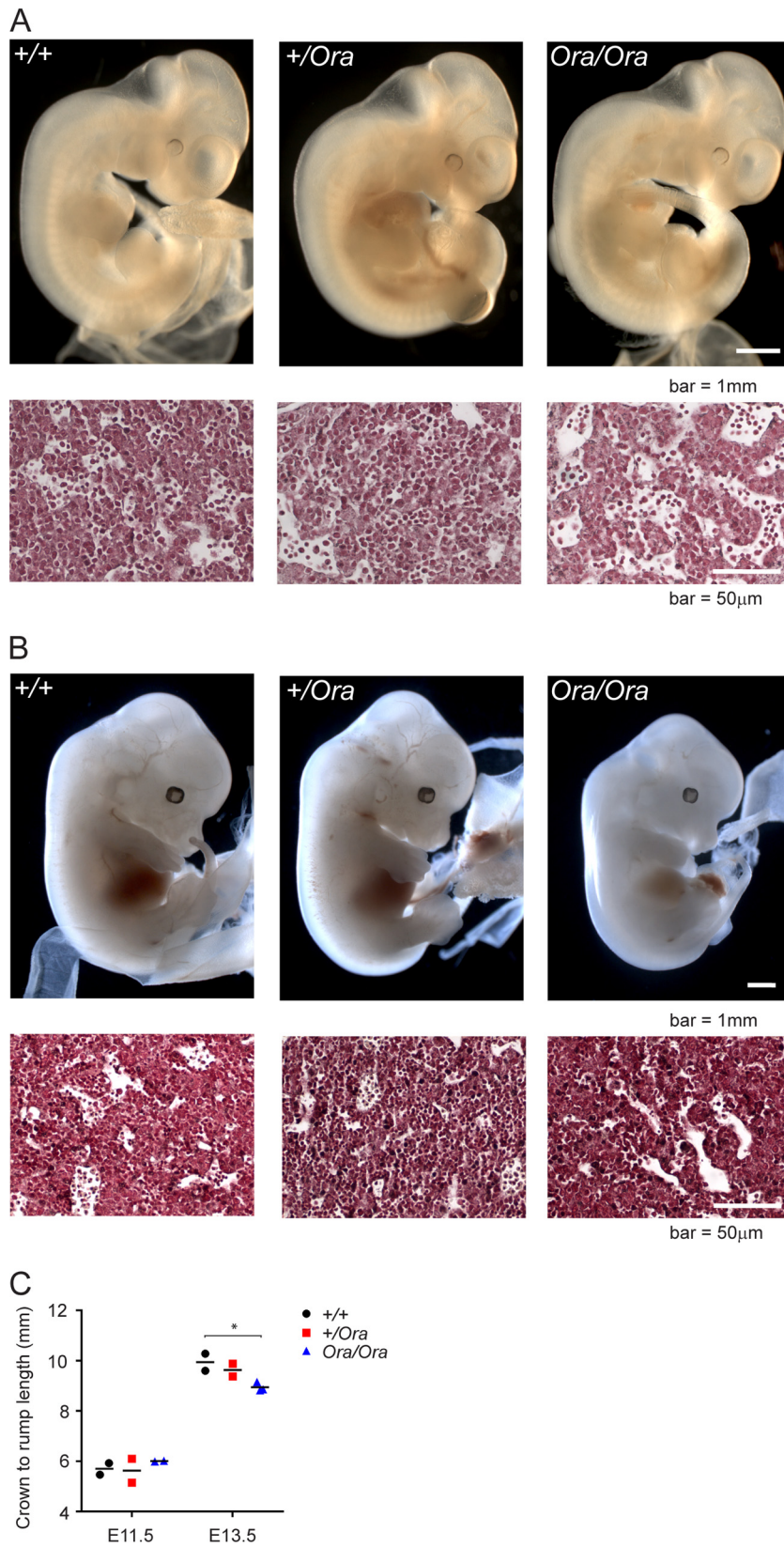
FIG 5 Reduced DHFR function leads to altered embryonic morphology and reduced erythrocyte production in the fetal liver. (A) Whole mounts of +/+, +/Ora, and Ora/Ora E11.5 embryos and corresponding neutral-red-stained fetal liver sections. (B) Whole mounts of +/+, +/Ora, and Ora/Ora E13.5 embryos and corresponding neutral-red-stained fetal liver sections. (C) Crown-to-rump measurements of E11.5 and E13.5 embryos. *, $P < 0.05$ (*t* test). The bars in the graph indicate the medians.
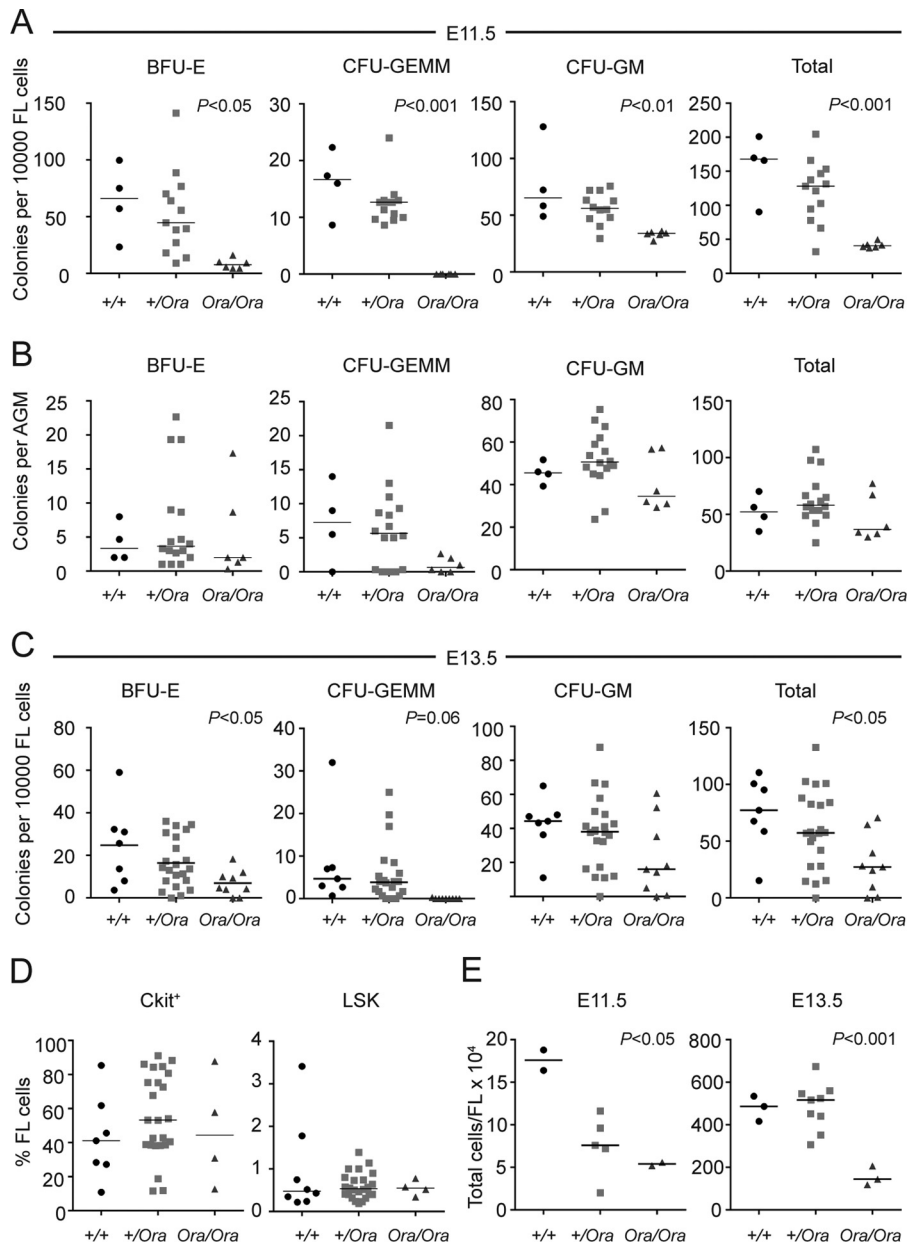
FIG 6 Reduced DHFR function leads to defects in embryonic blood production. (A and B) Functional assays of blood progenitors in E11.5 FL (A) and AGM (B). *P* values are indicated (one-way ANOVA). (C) Functional assays of blood progenitors in E13.5 FLs. *P* values are indicated (one-way ANOVA). (D) Flow cytometry analysis of cKit$^+$ and LSK cells in E13.5 FLs. (E) Total cells per FL at E11.5 and E13.5. *P* values are indicated (one-way ANOVA). The bars in the graphs indicate the medians.

CFU-GEMM colonies were also reduced in E13.5 Ora/Ora livers (Fig. 6C). These data suggest an early functional defect in both the erythroid and the most immature progenitor compartments. We also directly measured progenitor cells in E13.5 FLs and found that, while the number of functional progenitors was reduced, the percentage of cKit$^+$ and LSK cells in Ora/Ora livers was the same as in +/+ livers (Fig. 6D). Additionally, at both E11.5 and E13.5, the FLs of Ora/Ora embryos contained fewer cells than +/+ embryos (Fig. 6E). Together, these data indicate that definitive hematopoiesis is initiated in Ora/Ora mice and that blood progenitors successfully migrate to and colonize the FL, but they have a reduced capacity to undergo subse-

quent differentiation and expansion to form terminal blood types, particularly within the erythroid lineage.

Reduced DHFR leads to alterations in the erythroid compartment of resting and 5-fluorouracil-treated +/Ora mice. We then asked whether the small reduction in DHFR observed in +/Ora mice leads to phenotypic differences in adult mice. We first compared the numbers of a range of progenitor cells in the bone marrow of adult +/+ and +/Ora mice. Flow cytometric analysis indicated that MEPs, but not GMPs or CMPs, were reduced in +/Ora mice (Fig. 7A). Given this phenotype, the reduction in overall folate species in BM (Fig. 4C), our observations that BFU-E were
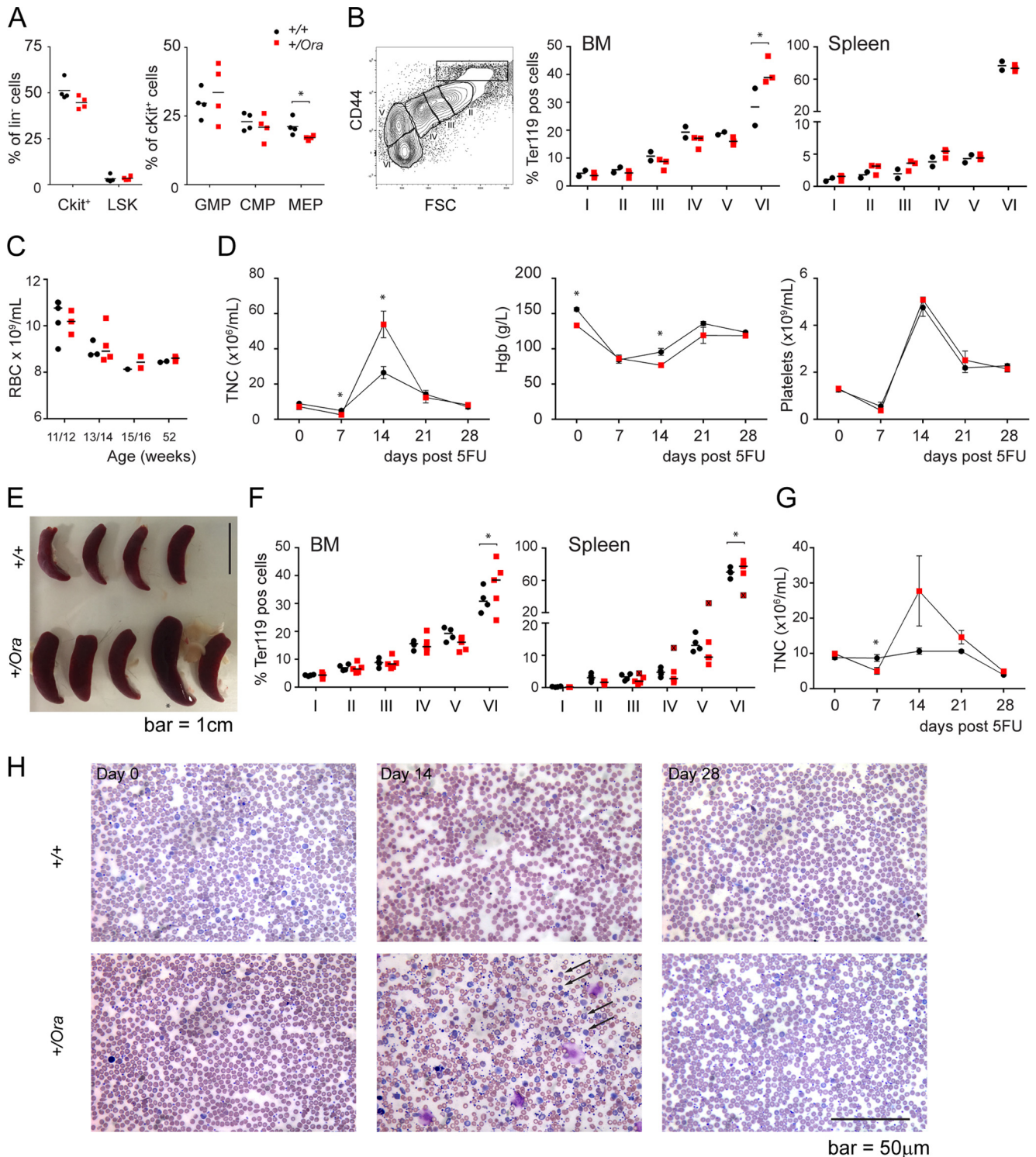
FIG 7 Reduced DHFR function leads to alterations in the erythroid compartment and impaired response to 5FU-induced hematoablation. (A) Flow cytometry analysis of blood progenitors in adult bone marrow. *, $P < 0.05$ (t test). The bars in all the graphs indicate the medians; each data point indicates an individual mouse. (B) Representative flow cytometry plot indicating gates used to determine maturing erythroid populations in panels B and F. The graphs show relative abundances of Ter119^{+} erythroid populations in BM and spleens of +/+ and +/Ora adult mice. *, $P < 0.05$ (t test). (C) Peripheral blood RBC counts in young and older +/+ and +/Ora mice. (D) Plots showing total TNC, Hgb, and platelets in peripheral blood (PB) of 8- to 9-month-old +/+ and +/Ora mice following 5FU treatment. *, $P < 0.05$ (t test). (E) Spleens of 8- to 9-month-old +/+ and +/Ora mice 28 days after 5FU treatment. The asterisk indicates the spleen from mouse 503. (F) Relative abundances of Ter119^{+} erythroid populations in BM and spleens of 8- to 9-month-old +/+ and +/Ora adult mice 28 days after 5FU treatment. *, $P < 0.05$ (t test). The data points from the spleen of mouse 503 (red squares marked with ×) were excluded from statistical analysis. (G) Plots showing TNC of 2- to 3-month-old +/+ and +/Ora mice following 5FU treatment. (H) Wright-stained PB smears from 2- to 3-month-old +/+ and +/Ora mice following 5FU treatment. The arrows indicate abundant nucleated red cells in the peripheral blood. The error bars indicate SEM.

reduced in Ora/Ora FLs at E11.5 and E13.5 (Fig. 6A and C), and the known requirement for folate in erythropoiesis (37), we asked whether erythroid maturation was altered in +/Ora mice. In the BM, there was a trend toward reduced proportions of nucleated erythroblasts (Fig. 7B, left graph, II to IV) and a significant increase in the proportion of mature erythrocytes (Fig. 7B, VI), suggesting that erythrocyte release is delayed in +/Ora mice. The gross spleen morphology was unchanged between +/+ and +/Ora mice (data not shown), but flow cytometry analysis of erythroid maturation showed a trend toward increased proportions of nucleated erythroblasts (Fig. 7B, right graph, I to IV). However, these changes did not translate to alterations in the number of circulating RBCs at any age (Fig. 7C).

We next asked whether we could reveal a more striking phenotype in +/Ora mice under conditions of stress hematopoiesis. We treated a cohort of older (8- to 9-month-old) +/+ and +/Ora mice with 5FU, which kills cycling hematopoietic cells but spares the quiescent HSCs, which are then stimulated into the cell cycle to repopulate the depleted marrow. As expected, total nucleated cells (TNC), hemoglobin (Hgb), and platelets dropped in the first 7 days after treatment and then recovered over the following 3 weeks (Fig. 7D). We observed a striking increase in TNC at day 14 in +/Ora mice compared to +/+ controls, which resolved by day 21 (Fig. 7D). At day 28, +/Ora mice had marked splenomegaly (Fig. 7E), highlighting the fact that +/Ora mice have prolonged extramedullary hematopoiesis. This splenomegaly was not observed in untreated mice of similar age (data not shown). Day 28 BM looked similar to the untreated controls (compare Fig. 7F to B). Despite the splenomegaly observed in the 5FU-treated +/Ora mice, the distributions of maturing erythroid cells in the spleen were similar between +/+ and +/Ora mice, with the exception of erythrocytes (Fig. 7F, VI) which were present in slightly higher numbers in the +/Ora mice.

We hypothesized that the increased nucleated cells observed in peripheral blood at day 14 were not leukocytes but rather nucleated red cells that appeared in the circulation in response to hematopoietic stress. To test this hypothesis, we treated an additional cohort of younger (2- to 3-month-old) +/+ and +/Ora mice with 5FU. We once again observed an increase in TNC at day 14 (Fig. 7G). Peripheral blood smears indicated a marked increase in nucleated red blood cells in +/Ora mice at day 14, consistent with the notion that +/Ora mice release immature nucleated red cells into the circulation under stress hematopoiesis conditions. Together, these data indicate that although +/Ora mice show mild changes in erythroid maturation at rest, these mice are able to produce normal numbers of circulating erythrocytes. However, following treatment with 5FU, +/Ora mice have perturbed erythropoiesis consistent with prolonged extramedullary hematopoiesis.

Reduced DHFR leads to impaired endothelium-dependent vasorelaxation in Orana mice, which can be restored by bolstering BH4 levels with sepiapterin. Along with its primary role in converting dietary folate to THF, DHFR has a secondary role in BH4 recycling, where it reduces BH2 to BH4 to maintain the homeostatic cellular BH4/BH2 ratio. This in turn prevents eNOS uncoupling and maintains NO bioactivity and endothelial function (Fig. 8A) (4, 38, 39). To examine the effect of DHFR deficiency on endothelial function in Orana mice, endothelium-dependent relaxation responses were measured in aortic rings from adult +/+ and +/Ora mice. Endothelium-dependent relaxation was significantly impaired in aortas from +/Ora mice compared to +/+ mice
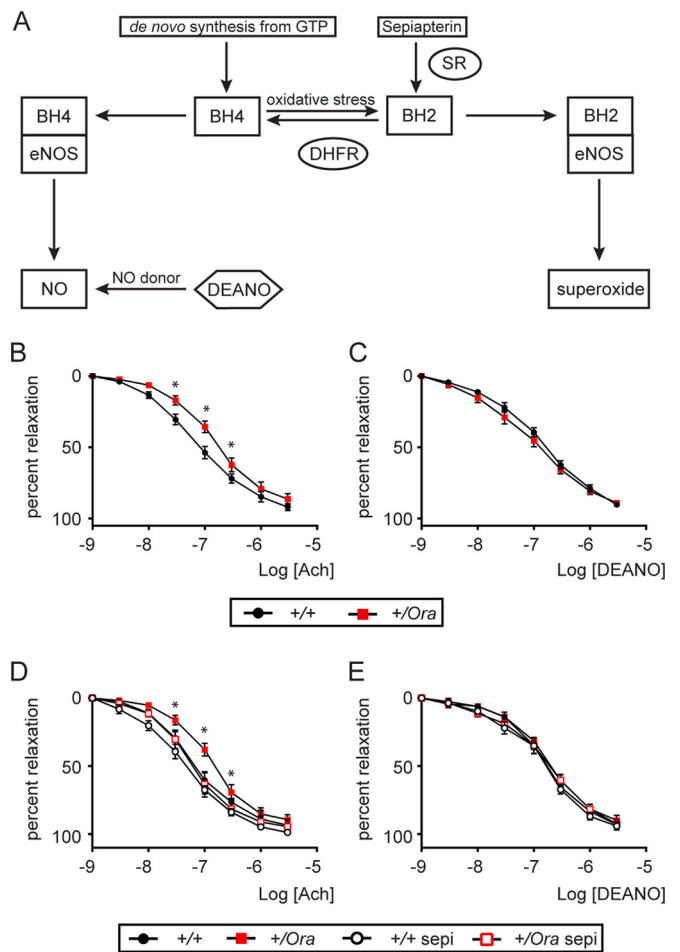

FIG 8 Reduced DHFR leads to impaired endothelium-dependent vasorelaxation in Orana mice, which can be restored by bolstering BH4 levels with sepiapterin. (A) Schematic representation of *de novo* BH4 synthesis and recycling pathways. BH4 is synthesized *de novo* from GTP via a series of reactions involving the rate-limiting enzyme GTPCH-1 and sepiapterin reductase (SR). BH4 is oxidized to BH2 in cells. DHFR can regenerate BH4 from BH2 via the recycling pathway. eNOS coupling is maintained when it is bound to BH4, producing NO, whereas BH2-bound eNOS leads to uncoupling and subsequent production of superoxide instead of NO. (B and C) Endothelium-dependent relaxation responses to Ach (B) and endothelium-independent relaxation responses to DEANO (C) of +/+ or +/Ora mice. The data are means ± SEM ($n = 5$). *, significant ($P < 0.05$) difference between +/+ and +/Ora aortic rings (unpaired t test). (D and E) Endothelium-dependent vasorelaxation responses to Ach (D) and endothelium-independent relaxation responses to DEANO (E) of +/+ or +/Ora mice in the absence or presence of sepiapterin (Sepi) (100 μmol/liter; 1 h preincubation). The data are means ± SEM ($n = 3$). *, significant ($P < 0.05$) difference between +/Ora and +/Ora Sepi aortic rings (unpaired t test). The relaxation responses to Ach or DEANO were recorded after vessel contraction with phenylephrine (300 nmol/liter).

(Fig. 8B). No significant difference was observed for endothelium-independent aortic relaxation induced by the NO donor DEANO (Fig. 8C and E), indicating that the relaxation defect observed in +/Ora mice was a result of altered endothelium-derived NO signaling and not an intrinsic defect in the aorta itself. Elevating vascular BH4 levels by preincubating vessels with sepiapterin restored endothelium-dependent relaxation responses in +/Ora mouse aortic rings to those seen in +/+ mice (Fig. 8D). These data verify that the endothelium in +/Ora aortas was dysfunctional, providing further

support for the previously described role of DHFR in maintaining endothelial BH4 levels through reduction of BH2 (38) and thereby preserving endothelium-dependent vasorelaxation responses.

DISCUSSION

In this study, we describe a mouse generated through an ENU mutagenesis screen that has a single point mutation in the *Dhfr* locus leading to a Thr136Ala substitution in the DHFR protein. Homozygote animals died of blood defects between E13.5 and E14.5, while heterozygote adults survived with a relatively intact blood compartment but showed tissue-specific defects in distribution of folate species and impaired vascular endothelial function. The Thr136Ala substitution is predicted to result in reduced affinity of DHFR for its substrate, consistent with our observation that the enzyme activity of recombinant DHFR^{Ora} was blunted. Interestingly, *in vitro* mutagenesis of Glu30, an amino acid that also forms a hydrogen bond with the pteridine moiety of folate (30, 32) and bonds directly to Thr136 (31, 32), produced a catalytically inactive form of DHFR (40). The Thr136Ala mutated version of the DHFR protein (DHFR^{Ora}) was barely detectable in either Ora/Ora mice or 293T cells transfected with a DHFR cDNA encoding the mutated version. Full-length and truncated versions of DHFR^{Ora} could be detected in transfected 293T cells treated with the proteasome inhibitor bortezomib, suggesting that DHFR^{Ora} was produced in cells but rapidly degraded.

Several families with mutations in the coding region of *DHFR* have been described in the literature. Individuals with deficiencies in DHFR are anemic and show various neurological symptoms (15, 16). Banka and colleagues (15) have described two apparently unrelated families in which infants presented with megaloblastic anemia and seizures. Subsequent genetic analysis in both families revealed a Leu80Phe substitution in DHFR, which is predicted to disrupt binding of the essential cofactor NADPH. However, Western blot analysis of an affected individual compared to controls and a heterozygote parent indicated that the DHFR protein was essentially absent in the homozygote. The lack of DHFR in these patients is similar to our findings with the Orana mouse, although the absence of DHFR appears to have less severe consequences in humans, since Ora/Ora mice die by E14.5. In contrast, affected humans survived into early childhood in cases where the DHFR deficiency was recognized and treated with folinic acid supplements. We attempted to rescue Ora/Ora pups with maternal folinic acid supplementation, but this did not yield an Ora/Ora neonate (data not shown). Interestingly, the proband in the first family was also identified as having low levels of BH4, but normal BH2, in the cerebrospinal fluid (CSF). This would be predicted to have effects on eNOS similar to those we describe here in +/Ora mice. A second family with an Asp153Val substitution has also been described (16). This mutation appears to be less disruptive to normal DHFR function than either Leu80Phe or Thr136Ala (Orana). DHFR protein was detectable at variable levels in all three affected patients; two patients with substantially lower DHFR both presented with childhood absence epilepsy and megaloblastic changes in the bone marrow.

A common feature in the human DHFR cases and our Orana mouse is defective blood production, as indicated by anemia in the human cases and reduced functional blood progenitors in Ora/Ora mice. Together, these data present a strong case for implicating DHFR as playing a role in definitive hematopoiesis. Our analysis of Ora/Ora embryos indicates a critical defect in hematopoietic progenitor expansion in the fetal liver. HSCs are initially formed in the AGM and then migrate to the FL, which is the primary embryonic hematopoietic organ from about

E11.5 (34–36). Functional progenitor cells were present in the AGM at E11.5, and flow cytometry analysis indicated that the progenitor cells migrated normally and were present in the FL at E13.5, despite having reduced capacity to expand. Thus, the DHFR-induced defect is not in blood formation *per se* but rather reflects an inability to expand progenitors and form the terminal blood cell types. We have not quantified whether the absolute numbers of HSCs generated by Ora/Ora mice are altered compared to +/+ mice; however, data from human patients with absent DHFR protein (identified in the postnatal period) combined with the data presented here suggest that the reduced DHFR primarily affects progenitor cell expansion rather than generation of HSCs *per se*. Further experimentation would be required to resolve whether the changes observed in FLs are cell autonomous or are a result of DHFR-dependent alterations in the surrounding microenvironment, as well as the progenitor cells themselves.

Our observations regarding embryonic blood production are consistent with the key role that DHFR plays in DNA synthesis and maintenance of DNA methylation, both of which are rate-limiting processes in cell proliferation. Although +/Ora mice have marginally reduced DHFR protein, hematopoietic progenitor expansion was similar to that in controls, while the adult mice had normal blood counts and only very mild changes in erythroid maturation at steady state. However, erythropoiesis was significantly perturbed under stress conditions in the +/Ora mice, with nucleated erythroblasts observed in the peripheral blood at day 14 following treatment with 5FU. It is unclear why the rapid proliferation of early embryogenesis is not impaired in Ora/Ora mice. Presumably, maternal folate stores are sufficient to maintain DNA synthesis and methylation through the early stages of embryogenesis but are inadequate to support extensive proliferation of blood progenitors by E13.5. This study also links DHFR deficiency to defective NO regulation in the vasculature. It is known that NO mediates HSC emergence from the AGM and perturbation of NO reduces hematopoietic potential *in vitro* and *in vivo* (41, 42). It is possible that the reduced progenitor expansion we observed in Ora/Ora embryos is due not only to compromised folate metabolism but also to effects of reduced DHFR on NO signaling in the AGM and the emergence of HSCs.

DHFR is critical for converting dietary folate into THF, and its downstream folate species are required for both DNA synthesis and methylation reactions. As expected, the distribution of folate species in Ora/Ora embryos was substantially altered, with a clear increase in the concentration of folic acid and a concomitant decrease in THF. Surprisingly, we did not observe differences in global DNA methylation in Ora/Ora embryos or differences in methylation within the CpG island of a known imprinted gene, which suggested that maternally derived folate was sufficient to maintain methyl donors (at least to E13.5). Even though we saw no changes in global DNA methylation, or methylation at the imprinted gene *Kcnq1ot1*, in either Ora/Ora embryos or +/Ora adults, we cannot rule out the possibility that the DHFR deficiency in Orana mice led to epigenetic changes at loci other than the one measured here. Previous studies have shown that there is no change in DNA methylation in either the erythroblasts of folate-deficient mice (37) or the BM of human patients with vitamin B$_{12}$ deficiency anemia (vitamin B$_{12}$ is required for conversion of 5-methyl THF to THF) (43).

Our investigations uncovered a number of hematopoietic changes in Ora/Ora and +/Ora mice compared to +/+ controls. These changes were largely centered on the erythroid compartment, which is consistent with the known requirements for folate in erythroid development (37). In +/Ora adults, erythroid maturation in both the BM and spleen was altered compared to +/+

mice. Specifically, we saw an overall reduction in nucleated erythroblasts in the BM and a concomitant increase in nucleated erythroblasts in the spleen. This phenotype is mild but suggests that the erythroid compartment is sensitive to even the small reduction in DHFR protein and subsequent reduction in folate concentration in the BM of +/Ora mice. These mice are able to compensate under steady-state conditions, possibly by increasing erythroid maturation in the spleen. A more striking phenotype became apparent in the +/Ora animals following treatment with 5FU, where we saw a large efflux of nucleated red cells into the circulation on day 14. Treatment with 5FU is known to damage the BM vasculature (44) and is likely to also damage the vasculature in other organs, including the spleen. Assuming that the +/Ora spleen continues to produce more nucleated red cells than +/+ controls following 5FU treatment (as observed at steady state), the increased nucleated red cells in the circulation of 5FU-treated +/Ora mice may be due to a combination of increased output from the spleen (and BM) and damaged vasculature with decreased capacity to regulate erythroblast release. Given that the +/Ora mice also have altered NO regulation in the vasculature (Fig. 8), it is likely that the combination of increased erythroblast production in the spleen, vascular damage, and altered endothelium-dependent vasorelaxation collectively produces the increased circulating nucleated erythroblasts. Alternatively, day 14 after 5FU treatment is the peak period of HSC mobilization, and this process may also involve release of erythroid cells into the circulation. Taking the data together, it is clear that while +/Ora mice can compensate for erythroid defects at steady state, their ability to increase hematopoiesis under stress conditions is compromised.

A feature of vascular diseases, such as diabetes, hypertension, and atherosclerosis, is endothelial dysfunction that manifests as a reduction in the bioactivity of NO produced by the endothelium. Considerable evidence has identified oxidative stress as an important cause of such endothelial dysfunction (6). More specifically, the endothelium from diseased vessels produces increased levels of $O_2^{\cdot-}$ that rapidly reacts with NO to form peroxynitrite, a reaction that impairs NO bioactivity (6). It is apparent that during disease, eNOS itself acts as a significant source of $O_2^{\cdot-}$ when its electron flow is "uncoupled" and O_2 accepts a terminal electron, generating $O_2^{\cdot-}$ instead of NO. A key determinant of eNOS coupling is the maintenance of a homeostatic BH4/BH2 ratio that is governed by the biosynthesis of BH4 by GTP-cylohydrolase-1 (GTPCH-1) and recycling of BH2 back to BH4 by DHFR (38). Thus, small interfering RNA (siRNA) inhibition of DHFR expression in endothelial cells elevates BH2 levels relative to BH4, with the increased BH2 capable of displacing eNOS-bound BH4, producing uncoupled eNOS, elevated $O_2^{\cdot-}$, and impaired NO bioactivity (4, 38, 39). Employing the novel Orana mouse, our data provide *in vivo* support for a key role for DHFR in the maintenance of endothelial BH4 levels, NO bioactivity, and endothelial function within intact mouse blood vessels. Thus, adult +/Ora mice exhibited impaired endothelium-dependent vasorelaxation in a manner that was reversed by bolstering BH4 levels via the *ex vivo* supplementation of aortas with the BH4 precursor sepiapterin. The finding that sepiapterin supplements effectively restored endothelial function in +/Ora mice suggests that although the *in vivo* deficiency in DHFR in Orana heterozygotes impairs NO bioactivity and endothelium-dependent relaxation, sufficient wild-type DHFR enzyme is available to convert excess *ex vivo* sepiapterin supplements into BH4 via the salvage pathway. These data are consistent with DHFR deficiency in +/Ora adult mice, resulting in an imbalance in the BH4/BH2 ratio, eNOS uncoupling, and impaired bioactivity of endothelium-derived NO.

The current study indicates that *in vivo* DHFR gene deficiency alone in mice impairs endothelial function in the absence of any cardiovascular disease or metabolic stress. DHFR expression levels are reduced in the aortas of diabetic mice (45, 46), angiotensin II-infused wild-type mice (47), BH4-deficient hph-1 mice, (48), ApoE gene knockout mice (49), and aged hypercholesterolemic LDL receptor gene knockout mice (50), which all correlates with reduced vascular BH4 levels and NO bioactivity. Where examined, restoration of DHFR levels via endothelium-targeted overexpression of the DHFR gene or folic acid supplements prevents eNOS uncoupling and inhibits the degree of hypertension or aortic aneurysm in Ang II-infused hph-1 (48) or ApoE gene knockout (49) mice and improves endothelial function in diabetic mice (46). Accordingly, the Orana heterozygote mouse represents a promising model to further define the *in vivo* role of DHFR in cardiovascular disease, similar to the hph-1 mouse also generated by ENU mutagenesis as a model of BH4 deficiency due to 90% constitutive reduction in GTPCH-1 activity (51). The hph-1 mouse has been instrumental in establishing the importance of GTPCH and BH4 in cardiac autonomic regulation (52) and protection against pulmonary hypertension (53, 54), *in vivo* eNOS uncoupling (55), and endothelial progenitor cell number and function during hypertension (56).

Orana mice should serve as a useful model for probing the *in vivo* function of DHFR, particularly its role in regulating NO signaling and its impact on hematopoietic stem cell emergence, erythroid maturation, and cardiovascular homeostasis. They will also be a useful tool to probe tissue- and locus-specific aberrations in DNA methylation and cancer susceptibility due to sustained defects in folate metabolism.

study design, data collection and interpretation, or the decision to submit the work for publication.

REFERENCES

1. **Liu JJ, Ward RL.** 2010. Folate and one-carbon metabolism and its impact on aberrant DNA methylation in cancer. Adv Genet **71:**79–121. http://dx.doi.org/10.1016/B978-0-12-380864-6.00004-3.
2. **Thony B, Auerbach G, Blau N.** 2000. Tetrahydrobiopterin biosynthesis, regeneration and functions. Biochem J **347:**1–16. http://dx.doi.org/10.1042/0264-6021:3470001.
3. **Werner-Felmayer G, Golderer G, Werner ER.** 2002. Tetrahydrobiopterin biosynthesis, utilization and pharmacological effects. Curr Drug Metab **3:**159–173. http://dx.doi.org/10.2174/1389200024605073.
4. **Chalupsky K, Cai H.** 2005. Endothelial dihydrofolate reductase: critical for nitric oxide bioavailability and role in angiotensin II uncoupling of endothelial nitric oxide synthase. Proc Natl Acad Sci U S A **102:**9056–9061. http://dx.doi.org/10.1073/pnas.0409594102.
5. **Vasquez-Vivar J, Kalyanaraman B, Martasek P, Hogg N, Masters BS, Karoui H, Tordo P, Pritchard KA, Jr.** 1998. Superoxide generation by endothelial nitric oxide synthase: the influence of cofactors. Proc Natl Acad Sci U S A **95:**9220–9225. http://dx.doi.org/10.1073/pnas.95.16.9220.
6. **Thomas SR, Witting PK, Drummond GR.** 2008. Redox control of endothelial function and dysfunction: molecular mechanisms and therapeutic opportunities. Antioxid Redox Signal **10:**1713–1765. http://dx.doi.org/10.1089/ars.2008.2027.
7. **Rajagopalan PT, Zhang Z, McCourt L, Dwyer M, Benkovic SJ, Hammes GG.** 2002. Interaction of dihydrofolate reductase with methotrexate: ensemble and single-molecule kinetics. Proc Natl Acad Sci U S A **99:**13481–13486. http://dx.doi.org/10.1073/pnas.172501499.
8. **Askari BS, Krajinovic M.** 2010. Dihydrofolate reductase gene variations in susceptibility to disease and treatment outcomes. Curr Genomics **11:**578–583. http://dx.doi.org/10.2174/138920210793360925.
9. **Johnson WG, Stenroos ES, Spychala JR, Chatkupt S, Ming SX, Buyske S.** 2004. New 19 bp deletion polymorphism in intron-1 of dihydrofolate reductase (DHFR): a risk factor for spina bifida acting in mothers during pregnancy? Am J Med Genet A **124A:**339–345. http://dx.doi.org/10.1002/ajmg.a.20505.
10. **Parle-McDermott A, Pangilinan F, Mills JL, Kirke PN, Gibney ER, Troendle J, O'Leary VB, Molloy AM, Conley M, Scott JM, Brody LC.** 2007. The 19-bp deletion polymorphism in intron-1 of dihydrofolate reductase (DHFR) may decrease rather than increase risk for spina bifida in the Irish population. Am J Med Genet A **143A:**1174–1180. http://dx.doi.org/10.1002/ajmg.a.31725.
11. **Gemmati D, De Mattei M, Catozzi L, Della Porta M, Serino ML, Ambrosio C, Cuneo A, Friso S, Krampera M, Orioli E, Zeri G, Ongaro A.** 2009. DHFR 19-bp insertion/deletion polymorphism and MTHFR C677T in adult acute lymphoblastic leukaemia: is the risk reduction due to intracellular folate unbalancing? Am J Hematol **84:**526–529. http://dx.doi.org/10.1002/ajh.21451.
12. **Morales C, Garcia MJ, Ribas M, Miro R, Munoz M, Caldas C, Peinado MA.** 2009. Dihydrofolate reductase amplification and sensitization to methotrexate of methotrexate-resistant colon cancer cells. Mol Cancer Ther **8:**424–432. http://dx.doi.org/10.1158/1535-7163.MCT-08-0759.
13. **Matherly LH, Taub JW, Ravindranath Y, Proefke SA, Wong SC, Gimotty P, Buck S, Wright JE, Rosowsky A.** 1995. Elevated dihydrofolate reductase and impaired methotrexate transport as elements in methotrexate resistance in childhood acute lymphoblastic leukemia. Blood **85:**500–509.
14. **Goker E, Waltham M, Kheradpour A, Trippett T, Mazumdar M, Elisseyeff Y, Schnieders B, Steinherz P, Tan C, Berman E.** 1995. Amplification of the dihydrofolate reductase gene is a mechanism of acquired resistance to methotrexate in patients with acute lymphoblastic leukemia and is correlated with p53 gene mutations. Blood **86:**677–684.
15. **Banka S, Blom HJ, Walter J, Aziz M, Urquhart J, Clouthier CM, Rice GI, de Brouwer AP, Hilton E, Vassallo G, Will A, Smith DE, Smulders YM, Wevers RA, Steinfeld R, Heales S, Crow YJ, Pelletier JN, Jones S, Newman WG.** 2011. Identification and characterization of an inborn error of metabolism caused by dihydrofolate reductase deficiency. Am J Hum Genet **88:**216–225. http://dx.doi.org/10.1016/j.ajhg.2011.01.004.
16. **Cario H, Smith DE, Blom H, Blau N, Bode H, Holzmann K, Pannicke U, Hopfner KP, Rump EM, Ayric Z, Kohne E, Debatin KM, Smulders Y, Schwarz K.** 2011. Dihydrofolate reductase deficiency due to a homozygous DHFR mutation causes megaloblastic anemia and cerebral folate deficiency leading to severe neurologic disease. Am J Hum Genet **88:**226–231. http://dx.doi.org/10.1016/j.ajhg.2011.01.007.
17. **Nguyen N, Judd LM, Kalantzis A, Whittle B, Giraud AS, van Driel IR.** 2011. Random mutagenesis of the mouse genome: a strategy for discovering gene function and the molecular basis of disease. Am J Physiol Gastrointest Liver Physiol **300:**G1–G11. http://dx.doi.org/10.1152/ajpgi.00343.2010.
18. **Papathanasiou P, Tunningley R, Pattabiraman DR, Ye P, Gonda TJ, Whittle B, Hamilton AE, Cridland SO, Lourie R, Perkins AC.** 2010. A recessive screen for genes regulating hematopoietic stem cells. Blood **116:**5849–5858. http://dx.doi.org/10.1182/blood-2010-04-269951.
19. **Aiso K, Nozaki T, Shimoda M, Kokue E.** 1999. Assay of dihydrofolate reductase activity by monitoring tetrahydrofolate using high-performance liquid chromatography with electrochemical detection. Anal Biochem **272:**143–148. http://dx.doi.org/10.1006/abio.1999.4174.
20. **Liu J, Hesson LB, Meagher AP, Bourke MJ, Hawkins NJ, Rand KN, Molloy PL, Pimanda JE, Ward RL.** 2012. Relative distribution of folate species is associated with global DNA methylation in human colorectal mucosa. Cancer Prev Res **5:**921–929. http://dx.doi.org/10.1158/1940-6207.CAPR-11-0577.
21. **Liu J, Pickford R, Meagher AP, Ward RL.** 2011. Quantitative analysis of tissue folate using ultra high-performance liquid chromatography tandem mass spectrometry. Anal Biochem **411:**210–217. http://dx.doi.org/10.1016/j.ab.2010.12.033.
22. **Quinlivan EP, Gregory JF III.** 2008. DNA methylation determination by liquid chromatography-tandem mass spectrometry using novel biosynthetic [U-15N]deoxycytidine and [U-15N]methyldeoxycytidine internal standards. Nucleic Acids Res **36:**e119. http://dx.doi.org/10.1093/nar/gkn534.
23. **Quinlivan EP, Gregory JF III.** 2008. DNA digestion to deoxyribonucleoside: a simplified one-step procedure. Anal Biochem **373:**383–385. http://dx.doi.org/10.1016/j.ab.2007.09.031.
24. **Umlauf D, Goto Y, Cao R, Cerqueira F, Wagschal A, Zhang Y, Feil R.** 2004. Imprinting along the Kcnq1 domain on mouse chromosome 7 involves repressive histone methylation and recruitment of Polycomb group complexes. Nat Genet **36:**1296–1300. http://dx.doi.org/10.1038/ng1467.
25. **Recipe.** 2009. Determination of homocysteine in plasma by LC-MSMS, p 90–91. ClinMass Application Note MS2000. Recipe, Munich, Germany. http://www.recipe.cz/recipe/katalog.pdf.
26. **Hempen C, Wanschers H, van der Sluijs Veer G.** 2008. A fast liquid chromatographic tandem mass spectrometric method for the simultaneous determination of total homocysteine and methylmalonic acid. Anal Bioanal Chem **391:**263–270. http://dx.doi.org/10.1007/s00216-008-1953-8.
27. **Lu C, Liu G, Jia J, Gui Y, Liu Y, Zhang M, Liu Y, Li S, Yu C.** 2011. Liquid chromatography tandem mass spectrometry method for determination of N-acetylcysteine in human plasma using an isotope-labeled internal standard. Biomed Chromatogr **25:**427–431. http://dx.doi.org/10.1002/bmc.1465.
28. **Li S, Jia J, Liu G, Wang W, Cai Y, Wang Y, Yu C.** 2008. Improved and simplified LC-ESI-MS/MS method for homocysteine determination in human plasma: application to the study of cardiovascular diseases. J Chromatogr B Analyt Technol Biomed Life Sci **870:**63–67. http://dx.doi.org/10.1016/j.jchromb.2008.06.003.
29. **Liu J, Zhang J, Ginzburg Y, Li H, Xue F, De Franceschi L, Chasis JA, Mohandas N, An X.** 2013. Quantitative analysis of murine terminal erythroid differentiation in vivo: novel method to study normal and disordered erythropoiesis. Blood **121:**e43–e49. http://dx.doi.org/10.1182/blood-2012-09-456079.
30. **Davies JF II, Delcamp TJ, Prendergast NJ, Ashford VA, Freisheim JH, Kraut J.** 1990. Crystal structures of recombinant human dihydrofolate reductase complexed with folate and 5-deazafolate. Biochemistry **29:**9467–9479. http://dx.doi.org/10.1021/bi00492a021.
31. **Oefner C, D'Arcy A, Winkler FK.** 1988. Crystal structure of human dihydrofolate reductase complexed with folate. Eur J Biochem **174:**377–385. http://dx.doi.org/10.1111/j.1432-1033.1988.tb14108.x.
32. **Bhabha G, Ekiert DC, Jennewein M, Zmasek CM, Tuttle LM, Kroon G, Dyson HJ, Godzik A, Wilson IA, Wright PE.** 2013. Divergent evolution of protein conformational dynamics in dihydrofolate reductase. Nat Struct Mol Biol **20:**1243–1249. http://dx.doi.org/10.1038/nsmb.2676.
33. **Banerjee RV, Matthews RG.** 1990. Cobalamin-dependent methionine synthase. FASEB J **4:**1450–1459.

34. **Medvinsky A, Dzierzak E.** 1996. Definitive hematopoiesis is autonomously initiated by the AGM region. Cell **86:**897–906. http://dx.doi.org/10.1016/S0092-8674(00)80165-8.

35. **Medvinsky AL, Samoylina NL, Muller AM, Dzierzak EA.** 1993. An early pre-liver intraembryonic source of CFU-S in the developing mouse. Nature **364:**64–67. http://dx.doi.org/10.1038/364064a0.

36. **Zovein AC, Hofmann JJ, Lynch M, French WJ, Turlo KA, Yang Y, Becker MS, Zanetta L, Dejana E, Gasson JC, Tallquist MD, Iruela-Arispe ML.** 2008. Fate tracing reveals the endothelial origin of hematopoietic stem cells. Cell Stem Cell **3:**625–636. http://dx.doi.org/10.1016/j.stem.2008.09.018.

37. **Koury MJ, Ponka P.** 2004. New insights into erythropoiesis: the roles of folate, vitamin B12, and iron. Annu Rev Nutr **24:**105–131. http://dx.doi.org/10.1146/annurev.nutr.24.012003.132306.

38. **Crabtree MJ, Tatham AL, Hale AB, Alp NJ, Channon KM.** 2009. Critical role for tetrahydrobiopterin recycling by dihydrofolate reductase in regulation of endothelial nitric-oxide synthase coupling: relative importance of the de novo biopterin synthesis versus salvage pathways. J Biol Chem **284:**28128–28136. http://dx.doi.org/10.1074/jbc.M109.041483.

39. **Sugiyama T, Levy BD, Michel T.** 2009. Tetrahydrobiopterin recycling, a key determinant of endothelial nitric-oxide synthase-dependent signaling pathways in cultured vascular endothelial cells. J Biol Chem **284:**12691–12700. http://dx.doi.org/10.1074/jbc.M809295200.

40. **Skacel N, Menon LG, Mishra PJ, Peters R, Banerjee D, Bertino JR, Abali EE.** 2005. Identification of amino acids required for the functional up-regulation of human dihydrofolate reductase protein in response to antifolate treatment. J Biol Chem **280:**22721–22731. http://dx.doi.org/10.1074/jbc.M500277200.

41. **North TE, Goessling W, Peeters M, Li P, Ceol C, Lord AM, Weber GJ, Harris J, Cutting CC, Huang P, Dzierzak E, Zon LI.** 2009. Hematopoietic stem cell development is dependent on blood flow. Cell **137:**736–748. http://dx.doi.org/10.1016/j.cell.2009.04.023.

42. **Adamo L, Naveiras O, Wenzel PL, McKinney-Freeman S, Mack PJ, Gracia-Sancho J, Suchy-Dicey A, Yoshimoto M, Lensch MW, Yoder MC, Garcia-Cardena G, Daley GQ.** 2009. Biomechanical forces promote embryonic haematopoiesis. Nature **459:**1131–1135. http://dx.doi.org/10.1038/nature08073.

43. **Ramsahoye BH, Burnett AK, Taylor C.** 1996. Nucleic acid composition of bone marrow mononuclear cells in cobalamin deficiency. Blood **87:**2065–2070.

44. **Hooper AT, Butler JM, Nolan DJ, Kranz A, Iida K, Kobayashi M, Kopp HG, Shido K, Petit I, Yanger K, James D, Witte L, Zhu Z, Wu Y, Pytowski B, Rosenwaks Z, Mittal V, Sato TN, Rafii S.** 2009. Engraftment and reconstitution of hematopoiesis is dependent on VEGFR2-mediated regeneration of sinusoidal endothelial cells. Cell Stem Cell **4:**263–274. http://dx.doi.org/10.1016/j.stem.2009.01.006.

45. **Oak JH, Cai H.** 2007. Attenuation of angiotensin II signaling recouples eNOS and inhibits nonendothelial NOX activity in diabetic mice. Diabetes **56:**118–126. http://dx.doi.org/10.2337/db06-0288.

46. **Youn JY, Gao L, Cai H.** 2012. The p47phox- and NADPH oxidase organiser 1 (NOXO1)-dependent activation of NADPH oxidase 1 (NOX1) mediates endothelial nitric oxide synthase (eNOS) uncoupling and endothelial dysfunction in a streptozotocin-induced murine model of diabetes. Diabetologia **55:**2069–2079. http://dx.doi.org/10.1007/s00125-012-2557-6.

47. **Gao L, Chalupsky K, Stefani E, Cai H.** 2009. Mechanistic insights into folic acid-dependent vascular protection: dihydrofolate reductase (DHFR)-mediated reduction in oxidant stress in endothelial cells and angiotensin II-infused mice: a novel HPLC-based fluorescent assay for DHFR activity. J Mol Cell Cardiol **47:**752–760. http://dx.doi.org/10.1016/j.yjmcc.2009.07.025.

48. **Gao L, Siu KL, Chalupsky K, Nguyen A, Chen P, Weintraub NL, Galis Z, Cai H.** 2012. Role of uncoupled endothelial nitric oxide synthase in abdominal aortic aneurysm formation: treatment with folic acid. Hypertension **59:**158–166. http://dx.doi.org/10.1161/HYPERTENSIONAHA.111.181644.

49. **Siu KL, Miao XN, Cai H.** 2014. Recoupling of eNOS with folic acid prevents abdominal aortic aneurysm formation in angiotensin II-infused apolipoprotein E null mice. PLoS One **9:**e88899. http://dx.doi.org/10.1371/journal.pone.0088899.

50. **Miller JD, Chu Y, Castaneda LE, Serrano KM, Brooks RM, Heistad DD.** 2013. Vascular function during prolonged progression and regression of atherosclerosis in mice. Arterioscler Thromb Vasc Biol **33:**459–465. http://dx.doi.org/10.1161/ATVBAHA.112.252700.

51. **Bode VC, McDonald JD, Guenet JL, Simon D.** 1988. hph-1: a mouse mutant with hereditary hyperphenylalaninemia induced by ethylnitrosourea mutagenesis. Genetics **118:**299–305.

52. **Adlam D, Herring N, Douglas G, De Bono JP, Li D, Danson EJ, Tatham A, Lu CJ, Jennings KA, Cragg SJ, Casadei B, Paterson DJ, Channon KM.** 2012. Regulation of beta-adrenergic control of heart rate by GTP-cyclohydrolase 1 (GCH1) and tetrahydrobiopterin. Cardiovasc Res **93:**694–701. http://dx.doi.org/10.1093/cvr/cvs005.

53. **Khoo JP, Zhao L, Alp NJ, Bendall JK, Nicoli T, Rockett K, Wilkins MR, Channon KM.** 2005. Pivotal role for endothelial tetrahydrobiopterin in pulmonary hypertension. Circulation **111:**2126–2133. http://dx.doi.org/10.1161/01.CIR.0000162470.26840.89.

54. **Nandi M, Miller A, Stidwill R, Jacques TS, Lam AA, Haworth S, Heales S, Vallance P.** 2005. Pulmonary hypertension in a GTP-cyclohydrolase 1-deficient mouse. Circulation **111:**2086–2090. http://dx.doi.org/10.1161/01.CIR.0000163268.32638.F4.

55. **Cosentino F, Barker JE, Brand MP, Heales SJ, Werner ER, Tippins JR, West N, Channon KM, Volpe M, Luscher TF.** 2001. Reactive oxygen species mediate endothelium-dependent relaxations in tetrahydrobiopterin-deficient mice. Arterioscler Thromb Vasc Biol **21:**496–502. http://dx.doi.org/10.1161/01.ATV.21.4.496.

56. **Xie HH, Zhou S, Chen DD, Channon KM, Su DF, Chen AF.** 2010. GTP cyclohydrolase I/BH4 pathway protects EPCs via suppressing oxidative stress and thrombospondin-1 in salt-sensitive hypertension. Hypertension **56:**1137–1144. http://dx.doi.org/10.1161/HYPERTENSIONAHA.110.160622.